Recursive Dictionary-Based Simultaneous Orthogonal Matching Pursuit for Sparse Unmixing of Hyperspectral Data

Kong Fanqiang *, *Guo Wenjun*, *Shen Qiu*, *Wang Dandan*

College of Astronautics, Nanjing University of Aeronautics and Astronautics, Nanjing 210016, P. R. China

(Received 29 September 2015; revised 7 March 2016; accepted 12 March 2016)

Abstract: The sparse unmixing problem of greedy algorithms still remains a great challenge at finding an optimal subset of endmembers for the observed data from the spectral library, due to the usually high correlation of the spectral library. Under such circumstances, a novel greedy algorithm for sparse unmixing of hyperspectral data is presented, termed the recursive dictionary-based simultaneous orthogonal matching pursuit (RD-SOMP). The algorithm adopts a block-processing strategy to divide the whole hyperspectral image into several blocks. At each iteration of the block, the spectral library is projected into the orthogonal subspace and renormalized, which can reduce the correlation of the spectral library. Then RD-SOMP selects a new endmember with the maximum correlation between the current residual and the orthogonal subspace of the spectral library. The endmembers picked in all the blocks are associated as the endmember sets of the whole hyperspectral data. Finally, the abundances are estimated using the whole hyperspectral data with the obtained endmember sets. It can be proved that RD-SOMP can recover the optimal endmembers from the spectral library under certain conditions. Experimental results demonstrate that the RD-SOMP algorithm outperforms the other algorithms, with a better spectral unmixing accuracy.

Key words: hyperspectral unmixing; greedy algorithm; simultaneous sparse representation; sparse unmixing

CLC number: TP751 **Document code**: A **Article ID**: 1005-1120(2017)04-0456-09

0 Introduction

Due to the low spatial resolution of the hyperspectral imaging sensor[1], each pixel in the hyperspectral image usually contains a mixture of several different materials. In order to deal with the problem of spectral mixing, hyperspectral unmixing is used to decompose each pixel's spectrum to identify and quantify the fractional abundances of the pure spectral signatures or endmembers in each mixed pixel[2]. In the past few years, the linear mixture model, which assumes that each mixed pixel is expressed as a linear combination of endmembers weighted by their corresponding abundances[3], has been widely applied for hyperspectral unmixing, due to its computational tractability and flexibility. Under the linear mixture model, several hyperspectral unmixing approaches based on geometry[4-5], statistics[6] and nonnegative matrix factorization[7] have been proposed. However, some of these methods[6-7] are unsupervised and could extract virtual endmembers with no physical meaning. Moreover, these methods are likely to fail if the pure pixel assumption is not fulfilled.

Sparse unmixing, as a semi-supervised linear spectral unmixing approach, has drawn many scholars' attention by now. Sparse unmixing has been proposed to model each mixed pixel in the hyperspectral image, which assumes that the observed image can be expressed as a linear combinations of spectral signatures from a large spectral library that is known in advance[3]. Several sparse regression techniques, such as greedy algorithms (GAs)[8,9], convex relaxation meth-

* Corresponding author, E-mail address: kongfq@nuaa.edu.cn.

How to cite this article: Kong Fanqiang, Guo Wenjun, Shen Qiu, et al. Recursive dictionary-based simultaneous orthogonal matching pursuit for sparse unmixing of hyperspectral data[J]. Trans. Nanjing Univ. Aero. Astro., 2017, 34(4): 456-464.

http://dx.doi.org/10.16356/j.1005-1120.2017.04.456

ods[10-13] and sparse Bayesian methods [14] are usually adopted to solve the sparse unmixing problem. Convex relaxation methods, such as spectral unmixing by variable splitting and augmented Lagrangian (SUnSAL)[11], SUnSAL-TV[12] and the constrained spectral unmixing by variable splitting and augmented Lagrangian (CLSUnSAL)[13], replace the l_0 norm with the l_1 norm, and use the alternating direction method of multipliers (ADMM) to solve the convex optimization problems. Convex relaxation methods can obtain the global sparse optimization solution and are more sophisticated than the greedy algorithms. However, convex relaxation methods cannot directly control the sparsity of the sparse optimization solution, since the number of endmembers participating in a mixed pixel is relatively small compared with the dimensionality of spectral library. The sparse Bayesian methods, such as Bayesian inference iterative conditional expectations (BI-ICE)[14], have been applied to the sparse unmixing problem. In Ref. [14], the unmixing problem is formulated as a hierarchical Bayesian inference problem, and priors for the model parameters. The BI-ICE method can obtain the sparse solution without tuning any parameters. However, it is much more complicated than the GAs and convex relaxation methods.

The greedy algorithms, such as orthogonal matching pursuit (OMP)[9], and matching pursuit (MP), can get an approximate solution for the l_0 norm problem without smoothing the penalty function and have low computational complexity. However, the greedy algorithms still remain a great challenge in finding the optimal subset of endmembers for the observed data from a large standard spectral library, without considering the spatial information. A major drawback of GAs is that GAs select one or more potential endmembers from the spectral library without considering the spatial information, which means it tends to be trapped into the local optimal solutions. To solve the local optimal solutions problem of GAs, several simultaneous greedy algorithms (SGAs), such as simultaneous orthogonal matching pursuit (SOMP)[15], simultaneous subspace pursuit (SSP)[16] and subspace matching pursuit (SMP)[16], were proposed. These SGAs adopt a block-processing strategy to divide the whole hyperspectral image into several blocks and pick some potential endmembers from the spectral library in each block. Then the endmembers picked in each block are associated as the optimal endmember sets of the whole hyperspectral data. SGAs can find the actual endmembers much more accurately than GAs but have the same low computational complexity as GAs. However, SGAs will adopt some nonexisting endmembers because of the usually high correlation of the spectral library, which adopts a block-processing strategy to select the potential endmembers. And the nonexisting endmembers will affect the spectral unmixing accuracy of SGAs.

Here, a novel algorithm is presented, termed the recursive dictionary-based simultaneous orthogonal matching pursuit (RD-SOMP), for sparse unmixing of hyperspectral data. RD-SOMP can be split into two steps: an endmember selection and an abundance estimation step. In the endmember selection step, similar to SOMP and SSP, RD-SOMP uses a block-processing strategy to divide the whole hyperspectral image into several blocks. In each block, the spectral library is projected into the orthogonal subspace and renormalized at each iteration, and then RD-SOMP selects the endmember with the maximum correlation between the current residual and the orthogonal subspace of the spectral library. In abundance estimation step, the abundances are estimated using the obtained endmember set under the constraint of nonnegativity.

1 Simultaneous Sparse Unmixing Model

The linear sparse unmixing model assumes that the observed spectrum of a mixed pixel is a linear combination of a few spectral signatures presented in a known spectral library. Let $y \in \mathbf{R}^L$ denote the measured spectrum vector of a mixed pixel with L bands, $\boldsymbol{A} \in \mathbf{R}^{L \times m}$ the $L \times m$ spectral library, with m being the number of signatures in

library $\boldsymbol{A}$. Hence, the linear sparse unmixing model can be expressed as [2]

$$y = \boldsymbol{A}x + n \tag{1}$$

where $x \in \mathbf{R}^m$ denotes the fractional abundance vector with regards to the library $\boldsymbol{A}$ and $n \in \mathbf{R}^L$ the noise and model error.

The simultaneous sparse unmixing model assumes that several input signals can be expressed as the different linear combinations of the same elementary signals. This means that, all the pixels in the hyperspectral image are constrained to share the same subset of endmembers selected from the spectral library. Then we can use SGA methods for sparse unmixing, the sparse unmixing model in Eq. (1) becomes

$$\boldsymbol{Y} = \boldsymbol{A}\boldsymbol{X} + \boldsymbol{N} \tag{2}$$

where $\boldsymbol{Y} \in \mathbf{R}^{L\times K}$ denotes the hyperspectral data matrix with L bands and K mixed pixels, $\boldsymbol{A} \in \mathbf{R}^{L\times m}$ the spectral library, $\boldsymbol{X} \in \mathbf{R}^{m\times K}$ the fractional abundance matrix, where each column represents the abundance fractions of a mixed pixel, and $\boldsymbol{N} \in \mathbf{R}^{L\times K}$ the noise matrix.

Under the simultaneous sparse unmixing model, the simultaneous sparse unmixing problem can be expressed as

$$\min_{X} \|\boldsymbol{X}\|_{\text{row}-0} \quad \text{s. t. } \|\boldsymbol{Y} - \boldsymbol{A}\boldsymbol{X}\|_{\text{F}} \leqslant \delta \tag{3}$$

where $\|\boldsymbol{X}\|_{\text{F}}$ denotes the Frobenius norm of $\boldsymbol{X}$, $\|\boldsymbol{X}\|_{\text{row}-0}$ the number of nonzero rows in the matrix $\boldsymbol{X}$, and δ the tolerated error due to the noise and model error.

2 Recursive Dictionary-Based Simultaneous Orthogonal Matching Pursuit

In this section, we first present our new algorithm, RD-SOMP, for sparse unmixing of hyperspectral data. Then, a theoretical analysis of the algorithm will be given.

2.1 Statement of algorithm

The whole process of RD-SOMP for sparse unmixing of hyperspectral data is summarized in Algorithm 1. The algorithm includes two main parts: endmember selection and abundance estimation. In the first part, we adopt a block-processing strategy for RD-SOMP to efficiently select endmembers. This strategy divides the whole hyperspectral image into several blocks. Then, in each block, RD-SOMP will select several potential endmembers from the spectral library and add them to the estimated endmember set. In the second part, the abundances are estimated using the obtained endmember set under the constraint of nonnegativity.

Algorithm 1 RD-SOMP for hyperspectral sparse unmixing

Part 1 (Endmember selection):

1: Initialize hyperspectral data $\boldsymbol{Y}$ and spectral library $\boldsymbol{A}$

2: Divide hyperspectral data $\boldsymbol{Y}$ into several blocks: $\boldsymbol{Y} = [Y_1, Y_2, \cdots, Y_B]$, and initialize the index set $S = \varnothing$, renormalized recursive matrix $\boldsymbol{\Psi} = \boldsymbol{A}$

3: For each block do

4: Set index set $S_b = \varnothing$ and iteration counter $k = 1$. Initialize the residual data of block b: $\boldsymbol{R}_0 = \boldsymbol{Y}_b$

5: While stopping criterion has not been met do

6: Compute the index of the best correlated member of $\boldsymbol{\Psi}$ to the actual residual: $j = \arg\max_i \|(\boldsymbol{R}^{l-1})^{\text{T}}\psi_i\|_2$, where ψ_i is the ith column of $\boldsymbol{\Psi}$

7: Update support set: $S_b = S_b \cup j$

8: Compute $X^l = \boldsymbol{A}_{S_b}^{\dagger} Y_b$ ($\boldsymbol{A}_{S_b}$ is the matrix containing the columns of $\boldsymbol{A}$ having the indexes from S_b, and $\boldsymbol{A}_{S_b}^{\dagger}$ is the pseudo-inverse of matrix $\boldsymbol{A}_{S_b}$. It is defined as $\boldsymbol{A}_{S_b}^{\dagger} = (\boldsymbol{A}_{S_b}^{\text{T}}\boldsymbol{A}_{S_b})^{-1}\boldsymbol{A}_{S_b}^{\text{T}}$.)

9: Update residual: $\boldsymbol{R}^l = \boldsymbol{Y}_b - \boldsymbol{A}_{S_b}\boldsymbol{X}^l$

10: $\boldsymbol{\Psi} = \boldsymbol{P}_{S_b}^{\perp}\boldsymbol{A}$ ($\boldsymbol{P}_{S_b}^{\perp}$ ($\boldsymbol{P}_{S_b}^{\perp} = \boldsymbol{I} - \boldsymbol{A}_{S_b}(\boldsymbol{A}_{S_b}^{\text{T}}\boldsymbol{A}_{S_b})^{-1}\boldsymbol{A}_{S_b}^{\text{T}}$) is the orthogonal projection matrix onto the range space of $\boldsymbol{A}_{S_b}$)

11: Renormalize $\psi_i = \psi_i / \|\psi_i\|_2$, for $i \notin S_b$

10: $l \leftarrow l + 1$

11: End while

12: Set $S = S \cup S_b$

13: End for

Part 2 (Abundance estimation): Estimate abundances using the original hyperspectral data

matrix and the endmember set under the constraint of nonnegativity.

$$\boldsymbol{X} \leftarrow \arg\min_{\boldsymbol{X}} \|\boldsymbol{A}_S\boldsymbol{X}-\boldsymbol{Y}\|_F \text{ , subject to } \boldsymbol{X} \geqslant 0$$

2.2 Notation

Here, we introduce some definitions, and then we give a theoretical analysis for the RD-SOMP algorithm.

Definition 1 If $\boldsymbol{x}$ is a vector, x_i the ith element of $\boldsymbol{x}$, the l_p norm of $\boldsymbol{x}$ is defined as

$$\|\boldsymbol{x}\|_p = \Big(\sum_i |x_i|^p\Big)^{\frac{1}{p}} \quad 1 \leqslant p < \infty \tag{4}$$

$$\|\boldsymbol{x}\|_\infty = \max_i |x_i| \tag{5}$$

Definition 2 The (p,q) operator norms of the matrix $\boldsymbol{A}$ is defined as

$$\|\boldsymbol{A}\|_{p,q} = \max_{x\neq 0} \frac{\|\boldsymbol{A}\boldsymbol{x}\|_q}{\|\boldsymbol{x}\|_p} \tag{6}$$

Several of the (p,q) operator norms can be computed easily using the following Lemma[15,17].

Lemma 1

(1) The $(1,q)$ operator norm is the maximum l_p norm of any column of $\boldsymbol{A}$.

(2) The $(2,2)$ operator norm is the maximum singular value of $\boldsymbol{A}$.

(3) The (p,∞) operator norm is the maximum l_p norm of any row of $\boldsymbol{A}$.

Definition 3 The cross-coherence parameter $\tilde{\mu}$ of a spectral library $\boldsymbol{A}$ and a renormalized recursive matrix $\boldsymbol{\Psi}$ equal the maximum correlation between two distinct atom[18]

$$\tilde{\mu} = \max_{m\neq h} |\langle \boldsymbol{A}_m, \boldsymbol{\psi}_h\rangle| \tag{7}$$

where $\boldsymbol{A}_m$ is the mth column of $\boldsymbol{A}$, $\boldsymbol{\psi}_h$ the hth column of $\boldsymbol{\Psi}$. If the cross-coherence parameter is small, each pair of $\boldsymbol{A}_m$ and $\boldsymbol{\psi}_h$ is nearly orthogonal.

Definition 4 The cumulative cross-coherence parameter[18] is defined as

$$\tilde{\mu}(K) = \max_{|\Lambda|\leqslant K} \max_{j\notin\Lambda} \sum_{i\in\Lambda} |\langle \boldsymbol{A}_i, \boldsymbol{\psi}_j\rangle| \tag{8}$$

where the index set Λ is the support of all the spectral signatures in the spectral library $\boldsymbol{A}$. The cumulative cross-coherence measures the maximum total correlation between a fixed atom library $\boldsymbol{\Psi}$ and K distinct spectral signatures. Particularly, $\tilde{\mu}(0)=0$.

2.3 Theoretical analysis

The simultaneous sparse unmixing problem in Eq. (3) is a NP-hard problem, which can be approximately solved using greedy algorithms or convex relaxation algorithms. For greedy algorithms, SOMP is used to approximately solve the optimization problem. Endmember selection and abundance estimation are the two main parts of SOMP. In the endmember selection step of SOMP, the endmembers in the joint support S are sequentially selected in the iterations. At nth iteration, an endmember is selected from the spectral library $\boldsymbol{A}$ which explains the smallest angle between the current residual $\boldsymbol{R}^{n-1}$ and the spectral library.

$$i = \arg\max_{i\notin\Omega^{n-1}} \|\boldsymbol{A}_i^{\mathrm{T}}\boldsymbol{R}^{n-1}\|_q$$
$$S^n = S^{n-1} \cup i \tag{9}$$

SOMP will recover a joint sparse representation with the support S whenever the exact recovery condition (ERC)[14] is met

$$\max_{j\notin S} \|\boldsymbol{A}_S^{\dagger}\boldsymbol{A}_j\|_1 < 1 \tag{10}$$

Different from endmember selection of SOMP, RD-SOMP selects the endmember with the smallest angle after the endmember is projected into the orthogonal subspace and renormalized at nth iteration.

$$i = \arg\max_{i\notin S^{n-1}} \|(\boldsymbol{\psi}_i^{(n-1)})^{\mathrm{T}}\boldsymbol{R}^{n-1}\|_q$$
$$\text{while } \boldsymbol{\psi}_l^{(n-1)} = \frac{\boldsymbol{P}_S^{\perp}\boldsymbol{A}_l}{\|\boldsymbol{P}_S^{\perp}\boldsymbol{A}_l\|_2} \tag{11}$$

where $\boldsymbol{P}_S^{\perp} = \boldsymbol{I} - \boldsymbol{A}_S(\boldsymbol{A}_S^{\mathrm{T}}\boldsymbol{A}_S)^{-1}\boldsymbol{A}_S^{\mathrm{T}}$.

To clarify the difference of the endmember selection process between SOMP and RD-SOMP, consider the situation of the endmember selection given in Fig. 1. Suppose $\boldsymbol{R}^{n-1}$ is the spectral vector of a mixed pixel, and it is constituted by two endmembers p_1 and p_2. SOMP selects the new endmember based on the least angle between the current residual and the endmembers. In Fig. 1, it would be p_3. RD-SOMP, on the contrary, selects the new endmember with the least angle between the current residual and the orthogonal subspace of the spectral library. It is clear that RD-SOMP will select p_1 instead of p_3.

Theorem 1 RD-SOMP will recover a joint

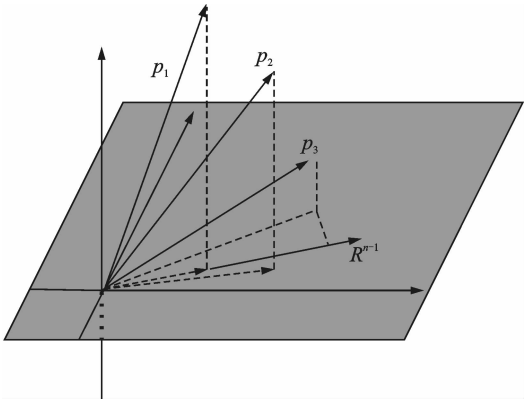

Fig. 1 Illustration of the flaw of endmember selection step

sparse representation with the support S whenever ERC is met.

$$\left\| (\boldsymbol{\Psi}_S^{\mathrm{T}}\boldsymbol{A}_S)^{-1}\boldsymbol{\Psi}_{\bar{S}}\boldsymbol{A}_S^{\mathrm{T}} \right\|_{1,1} \leqslant 1 \tag{12}$$

Proof According to $\boldsymbol{Y} = \sum_{i\in S}\boldsymbol{A}_i\boldsymbol{X}_i$, for the selection thresholding to select endmember in the support S, we need the inner product of signal with the corresponding atom $\boldsymbol{\psi}_l$ which is part of the support S to be larger than the inner product with any atom which is not part of the support S.

$$i \in S: |\langle \boldsymbol{\psi}_i, \boldsymbol{Y}\rangle| \geqslant |\langle \boldsymbol{\psi}_j, \boldsymbol{Y}\rangle|, \forall\, j \notin S \tag{13}$$

Concerning the fact that $\|\boldsymbol{X}\|_{1,\infty} \geqslant \|\boldsymbol{X}_i\|_1$, the inner product Eq. (13) can be rewritten as

$$i \in S: \|\boldsymbol{\psi}_i^{\mathrm{T}}\boldsymbol{Y}\|_1 \geqslant \|\boldsymbol{X}_i\|_1 |\langle \boldsymbol{\psi}_i, \boldsymbol{A}_i\rangle| - \sum_{k\in S, k\neq i}\|\boldsymbol{X}_j\|_1 |\langle \boldsymbol{\psi}_i, \boldsymbol{A}_k\rangle| \geqslant \|\boldsymbol{X}_i\|_1 |\langle \boldsymbol{\psi}_i, \boldsymbol{A}_i\rangle| - \|\boldsymbol{X}\|_{1,\infty}\sum_{k\in S, k\neq i}|\langle \boldsymbol{\psi}_i, \boldsymbol{A}_k\rangle| \tag{14}$$

$$j \notin S: \|\boldsymbol{\psi}_j^{\mathrm{T}}\boldsymbol{Y}\|_1 = \sum_{k\in S}\|\boldsymbol{X}_k\|_1 |\langle \boldsymbol{\psi}_j, \boldsymbol{A}_k\rangle| \leqslant \|\boldsymbol{X}\|_{1,\infty}\sum_{k\in S}|\langle \boldsymbol{\psi}_j, \boldsymbol{A}_k\rangle| \tag{15}$$

Using Definition 1, the above Eqs. (14, 15) can be simplified into

$$i \in S: \|\boldsymbol{\psi}_i^{\mathrm{T}}Y\|_1 \geqslant \|\boldsymbol{X}_i\|_1 |\langle \boldsymbol{\psi}_i, \boldsymbol{A}_i\rangle| - \|\boldsymbol{X}\|_{1,\infty}\tilde{\mu}(K-1) \tag{16}$$

$$k \notin S: \|\boldsymbol{X}\|_{1,\infty}\sum_{k\in S}|\langle \boldsymbol{\psi}_k, \boldsymbol{A}_j\rangle| = \|\boldsymbol{X}\|_{1,\infty}\tilde{\mu}(K) \tag{17}$$

Introducing Eqs. (16, 17) into Eq. (13), we can obtain

$$\frac{\|\boldsymbol{\psi}_i^{\mathrm{T}}\boldsymbol{Y}\|_1}{\|\boldsymbol{\psi}_k^{\mathrm{T}}\boldsymbol{Y}\|_1} \geqslant \frac{\|\boldsymbol{X}_i\|_1 |\langle \boldsymbol{\psi}_i, \boldsymbol{A}_i\rangle| - \|X\|_{1,\infty}\tilde{\mu}(K-1)}{\boldsymbol{X}_{1,\infty}\tilde{\mu}(K)} \geqslant 1 \tag{18}$$

As $\|\boldsymbol{X}\|_{1,\infty} \geqslant \|\boldsymbol{X}_i\|_1$, Eq. (18) can be rewritten as

$$|\langle \boldsymbol{\psi}_i, \boldsymbol{A}_i\rangle| \geqslant \frac{\|\boldsymbol{X}\|_{1,\infty}}{\|\boldsymbol{X}_i\|_1}(\tilde{\mu}(K-1) + \tilde{\mu}(K)) \geqslant \tilde{\mu}(K-1) + \tilde{\mu}(K) \tag{19}$$

After t iterations, t correct endmembers have been selected and the residual R_t is still a linear combination of the endmembers in the support S, i. e.

$$\boldsymbol{R}_t = \boldsymbol{A}_S\boldsymbol{C}_t \tag{20}$$

RD-SOMP will select a correct endmembers at the next iteration, if the maximum correlation between the residual R_t and the atom $\boldsymbol{\psi}_l$ which is in the support S is larger than the maximum correlation between $\boldsymbol{R}_t$ and any atom that is outside the support $\boldsymbol{I}$. So we can make sure that the expression satisfies

$$\frac{\max_{k\in\bar{I}}|\boldsymbol{\psi}_k^{\mathrm{T}}\boldsymbol{R}_t|}{\max_{i\in I}|\boldsymbol{\psi}_i^{\mathrm{T}}\boldsymbol{R}_t|} = \frac{\|\boldsymbol{\Psi}_I^{\mathrm{T}}\boldsymbol{R}_t\|_{1,\infty}}{\|\boldsymbol{\Psi}_I^{\mathrm{T}}\boldsymbol{R}_t\|_{1,\infty}} < 1 \tag{21}$$

Let $\boldsymbol{Z} = \boldsymbol{\Psi}_S^{\mathrm{T}}\boldsymbol{A}_S\boldsymbol{C}_t$, Eq. (21) can be rewritten as the following manner by using Lemma 1.

$$\frac{\|\boldsymbol{\Psi}_{\bar{S}}^{\mathrm{T}}\boldsymbol{A}_S\boldsymbol{C}_t\|_{1,\infty}}{\|\boldsymbol{\Psi}_S^{\mathrm{T}}\boldsymbol{A}_S\boldsymbol{C}_t\|_{1,\infty}} = \frac{\|\boldsymbol{\Psi}_{\bar{S}}^{\mathrm{T}}\boldsymbol{A}_S(\boldsymbol{\Psi}_S^{\mathrm{T}}\boldsymbol{A}_S)^{-1}\boldsymbol{Z}_{1,\infty}}{\boldsymbol{Z}_{1,\infty}} \leqslant \|\boldsymbol{\Psi}_{\bar{S}}^{\mathrm{T}}\boldsymbol{A}_S(\boldsymbol{\Psi}_S^{\mathrm{T}}\boldsymbol{A}_S)^{-1}\|_{\infty,\infty} \tag{22}$$

Using Lemma 1, Eq. (22) can be rewritten as

$$\|\boldsymbol{\Psi}_{\bar{S}}^{\mathrm{T}}\boldsymbol{A}_S(\boldsymbol{\Psi}_S^{\mathrm{T}}\boldsymbol{A}_S)^{-1}\|_{\infty,\infty} = \|(\boldsymbol{\Psi}_S^{\mathrm{T}}\boldsymbol{A}_S)^{-1}\boldsymbol{\Psi}_{\bar{S}}\boldsymbol{A}_S^{\mathrm{T}}\|_{1,1} \leqslant \|(\boldsymbol{\Psi}_S^{\mathrm{T}}\boldsymbol{A}_S)^{-1}\|_{1,1}\|\boldsymbol{\Psi}_{\bar{S}}\boldsymbol{A}_S^{\mathrm{T}}\|_{1,1} \tag{23}$$

To bound the first term of Eq. (23), the fact that whenever $\|\boldsymbol{D}\|_{1,1} < 1$ one has $\|(\boldsymbol{I}+\boldsymbol{D})^{-1}\|_{1,1} < (1-\|\boldsymbol{D}\|_{1,1})^{-1}$ is adopted.

Set $\boldsymbol{D} = \boldsymbol{\Psi}_S^{\mathrm{T}}\boldsymbol{A}_S - \boldsymbol{I}$, then

$$\|\boldsymbol{D}\|_{1,1} = \max_{i\in S}(|\langle \boldsymbol{\psi}_i, \boldsymbol{A}_i\rangle - 1| + \sum_{j\neq i}|\langle \boldsymbol{\psi}_j, \boldsymbol{A}_i\rangle|) \leqslant 1 - \min_{i\in S}|\langle \boldsymbol{\psi}_i, \boldsymbol{A}_i\rangle| + \tilde{\mu}(K-1) \tag{24}$$

Invoke Eq. (19) and Eq. (24), the first term of Eq. (23) can be rewritten as

$$\|(\boldsymbol{\Psi}_S^{\mathrm{T}}\boldsymbol{A}_S)^{-1}\|_{1,1} \leqslant \frac{1}{\min_{i\in S}|\langle \boldsymbol{\psi}_i, \boldsymbol{A}_i\rangle| - \tilde{\mu}(K-1)} \leqslant \frac{1}{\tilde{\mu}(K)} \tag{25}$$

Then the second term of Eq. (23) can be expressed as

$$\|\boldsymbol{\Psi}_{\bar{S}}\boldsymbol{A}_S^{\mathrm{T}}\|_{1,1} = \max_{k\in\bar{S}}\sum_{i\in S}|\langle \boldsymbol{\psi}_k, \boldsymbol{A}_i\rangle| \leqslant \tilde{\mu}_1(K) \tag{26}$$

Introducing Eqs. (25, 26) into Eq. (23), one

can attain

$$\| (\boldsymbol{\Psi}_S^{\mathrm{T}} \boldsymbol{A}_S)^{-1} \boldsymbol{\Psi}_{\bar{S}} \boldsymbol{A}_S^{\mathrm{T}} \|_{1,1} \leqslant 1 \tag{27}$$

This completes the argument.

3 Experiments

A simulated hyperspectral data set is used to demonstrate the performance of the proposed algorithm. In the experiment, the RD-SOMP algorithm is compared with two SGAs (SOMP[15], SMP[16]), and two convex relaxation methods (i.e., SUnSAL[11] and SUnSAL-TV[12]). The abundance nonnegativity constraint has been taken into account for all the algorithms. The TV regularizer used in SUnSAL-TV is a nonisotropic one. All the GAs have adopted the block-processing strategy to efficiently select actual endmembers. All the parameters of the test algorithms are tuned to their best performances.

The spectral library $\boldsymbol{A}$ used in the experiments is the United States Geological Survey (USGS) digital spectral library (splib06a)[19], which comprises 498 spectral signatures with reflectance values given in 224 spectral bands. Fifteen spectral signatures are chosen from the spectral library to generate the simulated data. Fig. 2 shows five spectral signatures used for the experiments. The other ten spectral signatures that are not displayed in Fig. 2 include Rhodochrosite HS67, Neodymium _ Oxide GDS34, Grossular WS484, Monazite HS255.3B, Meionite WS700.HLsep , Zoisite HS347.3B, Spodumene HS210.3B, Wollastonite HS348.3B, Rhodonite HS325.3B, and Pigeonite HS199.3B. The metric used to assess unmixing accuracy in all the experiments is the signal-to-reconstruction error (SRE)[9], which is used to measure the quality of the reconstruction abundances of spectral endmembers. SRE is defined as $\mathrm{SRE} \equiv \dfrac{E[\|\boldsymbol{x}\|_2^2]}{E[\|\boldsymbol{x}-\hat{\boldsymbol{x}}\|_2^2]}$, and measured in unit decibel: $\mathrm{SRE(dB)} \equiv 10\log_{10}(\mathrm{SRE})$. In general, the larger the SRE, the closer the estimation of the truth.

In the experiments, six data sets of 50 pixel × 50 pixel and 224 bands per pixel are generated, which contain a different number of endmembers: 5, 7, 9, 11, 13, 15. In each simulated pixel, the fractional abundances of the endmembers are randomly generated, following a Dirichlet distribution[13]. Note that there is no pure pixel in simulated data 1, and the fractional abundances of the endmembers are less than 0.8. After simulated data 1 is generated, correlated noise or Gaussian white noise is added to simulated data 1, having different levels of the signal-to-noise ratio ($\mathrm{SNR} \equiv 10\log_{10}(\dfrac{\|\boldsymbol{Ax}\|_2^2}{\|\boldsymbol{n}\|_2^2})$). The Gaussian white noise is generated using the AWGN function in MATLAB. The correlated noise is obtained by low-pass filtering i.i.d. Gaussian noise.

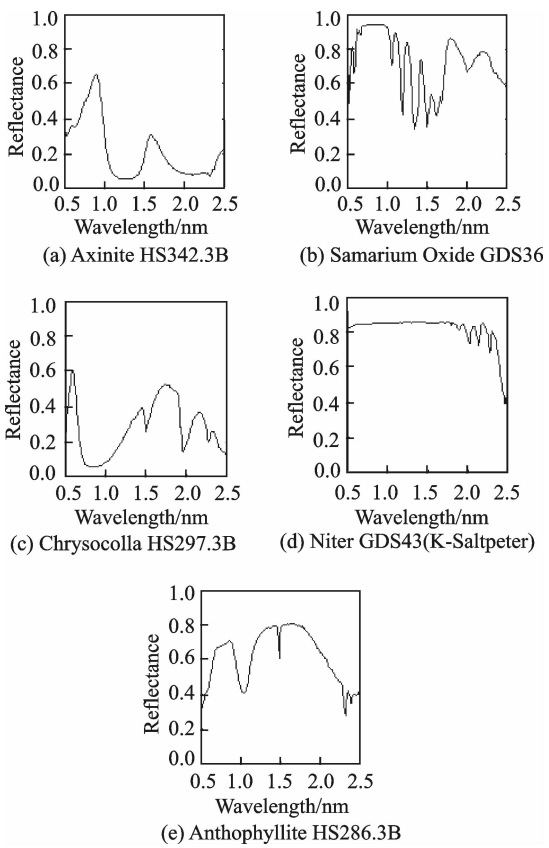

Fig. 2 Five spectral signatures from USGS used in our simulated data experiments

Figs. 3, 4 show the SRE results as a function of endmember number obtained using different test methods. The SREs of all the test methods decrease when the endmember number increases. RD-SOMP, SOMP, SMP, and SUnSAL-TV perform better than SUnSAL. Among all the methods, RD-SOMP and SMP behave better than the other methods, and RD-SOMP can always obtain

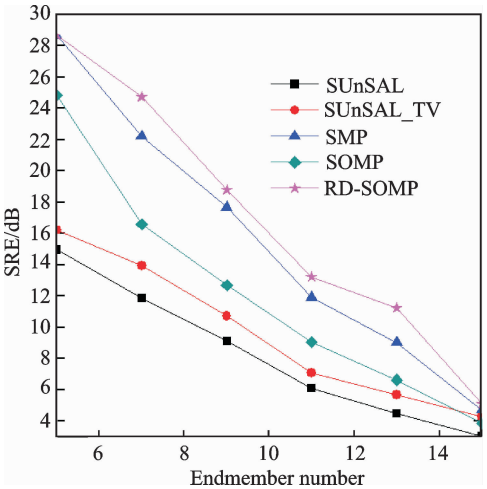

Fig. 3 Results of the simulated data with 30 dB white noise (SRE as function of endmember number)

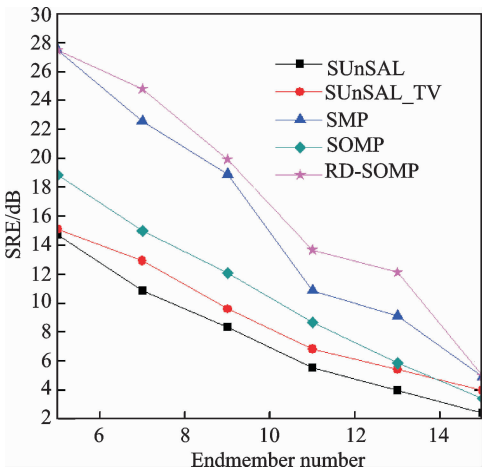

Fig. 4 Results of the simulated data with 30 dB correlated noise (SRE as function of endmember number)

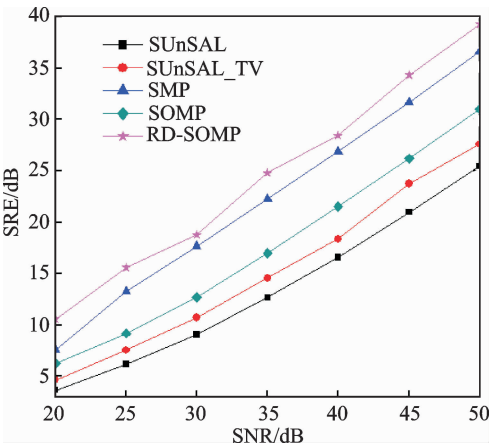

Fig. 5 Results of the simulated data with white noise when endmember number is nine (SRE as function of SNR)

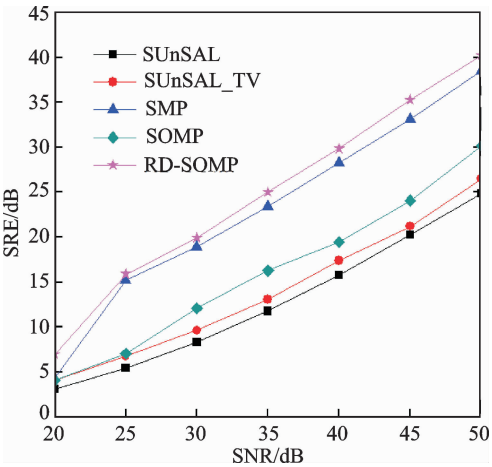

Fig. 6 Results of the simulated data with correlated noise when the endmember number is nine (SRE as function of SNR)

the best result. Fig. 5 and Fig. 6 show the SRE as a function of SNR when the endmember number is nine. The SREs of the test methods decrease with the decrease of SNR. As shown in Fig. 5 and Fig. 6, all the SGA methods are superior to SUnSAL and SUnSAL-TV. The result indicates that, all the SGA methods adopt the block-processing strategy to effectively pick up all the actual endmembers. Amongst all the SGA methods, RD-SOMP achieves an overall optimal performance.

Fig. 7 shows the number of potential endmembers obtained from the spectral library using all the SGA methods. RD-SOMP can select the actual endmembers more accurately than SOMP and SMP. All the GAs have adopted the block-processing strategy to efficiently select actual endmembers. Here, we discuss how to properly set the block size for all the GAs. In general, in the same simulated data experiment, the number of selected endmembers by a GA algorithm will decrease as the block size increases. However, a large block size causes missing of some actual endmembers. Note that the block sizes set of all the GAs is different but tuned to their best performances to achieve the optimal results. It is worth mentioning that the nonexisting endmembers in the estimated endmember set will have a negative effect on the reconstruction of the abundances corresponding to the actual endmembers. RD-SOMP selects a new endmember from the or-

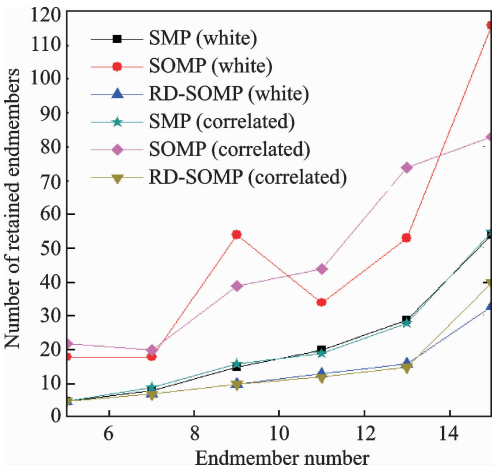

Fig. 7 Results obtained by three SGA methods on the simulated data with 30 dB white noise or correlated noise (Number of retained endmembers as function of endmember number)

thogonal subspace of the spectral library at each iteration, which can select the actual endmembers more accurately than SOMP and SMP. It indicates that RD-SOMP performs better than both SOMP and SMP.

Table 1 shows the processing time measured after applying the tested algorithms to the simulated data with 30 dB white noise. The algorithms are implemented in MATLAB 2009a and executed on a desktop PC with an Intel Core (TM) i5 CPU (3.2 GHz) and 4 GB of DRAM memory. RD-SOMP, SOMP and SMP have similar computational complexity while the SUnSAL-TV algorithm is far more time-consuming compared with the other algorithms.

Table 1 Processing time (s) measured after applying the tested methods to simulated data with 30 dB white noise

Data cube	SUnSAL	SUnSAL-TV	SOMP	SMP	RD-SOMP
Simulated data	43.07	142.26	8.096	8.225	5.903

4 Conclusions

A new greedy algorithm is presented, termed the RD-SOMP for sparse unmixing of hyperspectral data. In the existing SGA methods, endmember selection and abundance estimation are two main parts. In the endmember selection step, the endmember selection criterion of RD-SOMP is different from SOMP and SMP. SOMP and SMP select a new endmember with the least angle between the current residual and the spectral library, while RD-SOMP firstly projects the spectral library into the orthogonal subspace and renormalizes it to reduce the correlation of the spectral library, and then RD-SOMP selects a new endmember according to the maximum correlation between the current residual and the orthogonal subspace of the spectral library. Thus, RD-SOMP can select the actual endmembers more accurately than SOMP and SMP. It is obvious that the more accurately the actual endmembers are selected, the better the abundances will be estimated. Experiments on the simulated data also demonstrate that the RD-SOMP algorithm is more effective for sparse unmixing than other SGA algorithms.

Acknowledgments

This work was supported by the National Natural Science Foundations of China (Nos. 61401200, 61201365).

References:

[1] KONG F, JING Q, JI Z. Compressed sensing reconstruction algorithm of interferometric multi-spectral image based on interframe prediction and joint optimization[J]. Journal of Nanjing University of Aeronautics and Astronautics, 2013, 45(2):225-231. (in Chinese)

[2] KESHAVA N, MUSTARD J F. Spectral unmixing [J]. IEEE Signal Processing Mag, 2002, 19(1):44-57.

[3] BIOUCAS-DIAS J M, PLAZA A, DOBIGEON N, et al. Hyperspectral unmixing overview: Geometrical, statistical, and sparse regression-based approaches[J]. Selected Topics in Applied Earth Observations and Remote Sensing, IEEE Journal of, 2012, 5(2): 354-379.

[4] MIAO L, QI H. Endmember extraction from highly mixed data using minimum volume constrained nonnegative matrix factorization[J]. IEEE Trans Geosci Remote Sens, 2007, 45(3): 765-777.

[5] CHAN T, CHI C, HUANG Y, et al. A convex analysis-based minimum-volume enclosing simplex algorithm for hyperspectral unmixing[J]. IEEE Trans

Signal Process, 2009, 57(11): 4418-4432.

[6] ARNGREN M, SCHMIDT M N, LARSEN J. Bayesian nonnegative matrix factorization with volume prior for unmixing of hyperspectral images[C]// Proc IEEE Int Workshop MLSP. France: Grenoble, 2009: 1-6.

[7] QIAN Y, JIA S, ZHOU J, et al. Hyperspectral unmixing via sparsity-constrained nonnegative matrix factorization[J]. IEEE Trans Geosci Remote Sens, 2011, 49(11): 4282-4297.

[8] YAN X, ZHANG L, GUO W. Dual-sparsity preserving projection[J]. Transactions of Nanjing University of Aeronautics & Astronautics, 2012(3):90-94.

[9] IORDACHE M D, BIOUCAS-DIAS J M, PLAZA A. Sparse unmixing of hyperspectral data[J]. IEEE Trans Geosci Remote Sens, 2011, 49(6): 2014-2039.

[10] WANG C, KONG Y. Radar high-resolution range profile target recognition based on sparse representation of dictionary optimized[J]. Journal of Nanjing University of Aeronautics & Astronautics, 2013, 45(6):837-842. (in Chinese)

[11] AFONSO M V, BIOUCAS-DIAS J M, FIGUEIREDO M A T. An augmented Lagrangian approach to the constrained optimization formulation of imaging inverse problems[J]. IEEE Trans Image Process, 2011, 20(3): 681-695.

[12] IORDACHE M D, BIOUCAS-DIAS J M, PLAZA A. Total variation spatial regularization for sparse hyperspectral unmixing[J]. IEEE Trans Geosci Remote Sens, 2012, 50(11): 4484-4502.

[13] IORDACHE M D, BIOUCAS-DIAS J M, PLAZA A. Collaborative sparse regression for hyperspectral unmixing[J]. IEEE Trans Geosci Remote Sens, 2014, 52(1): 341-354.

[14] THEMELIS K E, RONTOGIANNIS A A, KOUTROUMBAS K D. A novel hierarchical Bayesian approach for sparse semisupervised hyperspectral unmixing[J]. IEEE Trans Signal Process, 2012, 60(2): 585-599.

[15] TROPP J A, GILBERT A C, STRAUSS M J. Algorithms for simultaneous sparse approximation. Part I: Greedy pursuit[J]. Signal Processing, 2006, 86(3): 572-588.

[16] SHI Z, TANG W, DUREN Z, et al. Subspace matching pursuit for sparse unmixing of hyperspectral data[J]. IEEE Trans Geosci Remote Sens, 2014, 52(6): 3256-3274.

[17] CHEN J, HUO X. Theoretical results on sparse representations of multiple-measurement vectors[J]. IEEE Trans Signal Process, 2006, 54(12): 4634-4643.

[18] SCHNASS K, VANDERGHEYNST P. Dictionary preconditioning for greedy algorithms[J]. IEEE Trans Signal Process, 2008, 56(5): 1994-2002.

[19] CLARK R N, SWAYZE G A, WISE R, et al. USGS digital spectral library splib06a[M]. Denver, CO, USA: U. S. Geological Survey, 2007.

Dr. **Kong Fanqiang** is currently a lecturer at the College of Astronautics, Nanjing University of Aeronautics and Astronautics (NUAA), Nanjing, China. He received his Ph. D. degree in information and communication engineering from Xidian University, Xi'an, China, in 2008. His research interests focus on spectral image coding and image analysis, artificial intelligence, and pattern recognition.

Mr. **Guo Wenjun** received his M. S. degree in communication and information system from NUAA, Nanjing, China, in 2016. His current research interests focus on hyperspectral remote sensing image processing and sparse representation.

Dr. **Shen Qiu** is currently a lecturer at the College of Astronautics in NUAA, Nanjing, China. She received her Ph. D. degree in information and communication engineering from University of Science and Technology of China, He'fei, China, in 2009. Her research interests focus on artificial intelligence and pattern recognition.

Ms. **Wang Dandan** received the M. S. degree in communication and information system from NUAA, Nanjing, China, in 2017. Her current research interests focus on hyperspectral remote sensing image processing and sparse representation.

(Executive Editor: Zhang Tong)